PAPER • OPEN ACCESS

Group velocity matching in high-order harmonic generation driven by mid-infrared lasers

To cite this article: C Hernández-García *et al* 2016 *New J. Phys.* **18** 073031

View the article online for updates and enhancements.

Related content

- Macroscopic aspects of attosecond pulse generation
  Mette B Gaarde, Jennifer L Tate and Kenneth J Schafer

- Tailoring isolated attosecond pulses using quantum path interferences
  Carlos Hernández-García and Luis Plaja

- Recent progress of below-threshold harmonic generation
  Wei-Hao Xiong, Liang-You Peng and Qihuang Gong

Recent citations

- Bright, high-repetition-rate water window soft X-ray source enabled by nonlinear pulse self-compression in an antiresonant hollow-core fibre
  M. Gebhardt *et al*

- Transverse phase matching of high-order harmonic generation in single-layer graphene
  Roberto Boyero-García *et al*

- Attosecond light science and its application for probing quantum materials
  Xun Shi *et al*

New Journal of Physics

The open access journal at the forefront of physics

PAPER

CrossMark

Group velocity matching in high-order harmonic generation driven by mid-infrared lasers

C Hernández-García[1,2], T Popmintchev[1], M M Murnane[1], H C Kapteyn[1], L Plaja[2], A Becker[1] and A Jaron-Becker[1]

[1] JILA and Department of Physics, University of Colorado at Boulder, Boulder, CO 80309-0440, USA
[2] Grupo de Investigación en Aplicaciones del Láser y Fotónica, University of Salamanca E-37008, Salamanca, Spain

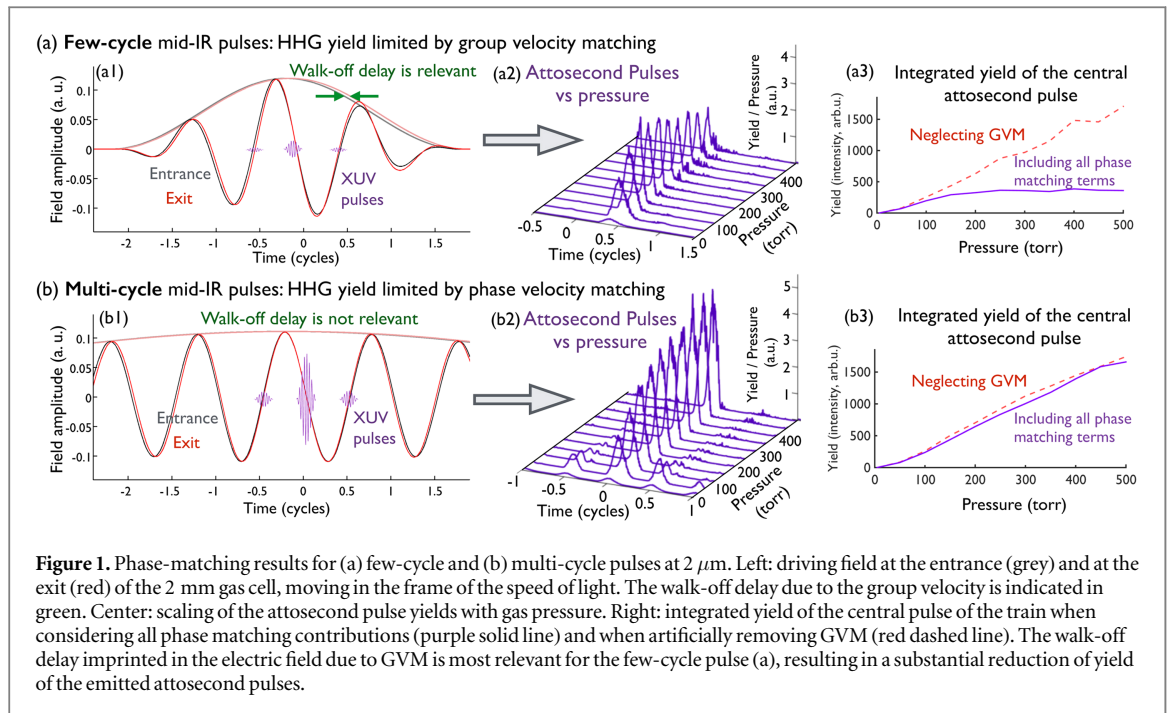E-mail: carloshergar@usal.es

Abstract

We analyze the role of group-velocity matching (GVM) in the macroscopic build up of the high-harmonic signal generated in gas targets at high pressures. A definition of the walk-off length, associated with GVM, in the non-perturbative intensity regime of high-harmonic generation is given. Semiclassical predictions based on this definition are in excellent agreement with full quantum simulations. We demonstrate that group velocity matching is a relevant factor in high harmonic generation and the isolation of attosecond pulses driven by long wavelength lasers and preferentially selects contributions from the short quantum trajectories.

1. Introduction

High-order harmonic generation (HHG) is a unique source of coherent radiation extending from the extreme-ultraviolet (EUV) to the soft x-ray regime [1–3]. HHG radiation is emitted in form of attosecond light pulses [4–6] and, under specific conditions even as waveforms on the zeptosecond time scale [7]. Microscopically, HHG can be understood by a semiclassical three-step model [8, 9]: an electron tunnels from an atom or molecule by interacting with an intense laser field, then it is accelerated, and finally driven back by the field to its parent ion, releasing the excess energy in the form of radiation upon recombination into the initial state. In each half-cycle, two electron trajectories, termed as short and long according to their excursion time, lead to recollisions of the same kinetic energy, and hence give rise to the same harmonic.

Macroscopically, the HHG signal results from the coherent superposition of the fields emitted from each atom in the target. Thus, the detected harmonic signal strongly depends on the phase acquired from the fundamental field and from the HHG process itself [10, 11]. The difference in phase and group velocities of the fundamental and harmonic fields as they propagate through the generating medium, leads to a phase and a group-velocity mismatch, respectively. In HHG using Ti:Sapphire driving lasers at 800 nm, the phase–velocity mismatch dominates because high single-atom yield and high gas dispersion allow for HHG at relative low gas pressures (<1 atm over extended distances). To generate bright coherent EUV HHG beams, phase–velocity mismatch due to dispersion from neutral atoms and plasma, together with contributions resulting from the intrinsic phase of the HHG process [12–14] and the geometry (e.g. waveguide or Gouy phase), can be balanced. This process is usually termed phase matching [15]. Good phase matching can also be achieved for HHG driven with mid-infrared (mid-IR) driver pulses [3, 16–18]. However, in order to achieve a large HHG efficiency at these long wavelengths, high gas pressures must be used to overcome the low single-atom yield. As a result, group velocity matching (GVM) between the fundamental and HHG fields is expected to play a role as well. Simple analytic calculations for extreme nonlinear HHG driven by mid-IR lasers suggest that the GVM between the fundamental and the higher-order harmonics can be significant [16, 19].

Previously, the GVM effect has only been considered in perturbative second harmonic generation (SHG) in crystals. There, it has long been recognized that GVM between the fundamental and second harmonic fields has an important effect on the conversion efficiency and pulse broadening of ultrashort laser pulses [20, 21].

Figure 1. Phase-matching results for (a) few-cycle and (b) multi-cycle pulses at 2 μm. Left: driving field at the entrance (grey) and at the exit (red) of the 2 mm gas cell, moving in the frame of the speed of light. The walk-off delay due to the group velocity is indicated in green. Center: scaling of the attosecond pulse yields with gas pressure. Right: integrated yield of the central pulse of the train when considering all phase matching contributions (purple solid line) and when artificially removing GVM (red dashed line). The walk-off delay imprinted in the electric field due to GVM is most relevant for the few-cycle pulse (a), resulting in a substantial reduction of yield of the emitted attosecond pulses.

Accurate models to account for GVM in the perturbative interaction regime have thus been developed [22–24]. In this paper we implement 3D quantum simulations of mid–IR driven HHG to compare the magnitude of the phase slips due to group and phase velocity mismatch, as well as other geometric effects. We find that GVM effects are large at long driver wavelengths and for short pulses, motivating a new definition of the group velocity walk-off length that is valid for the extreme non-perturbative nonlinear optics of HHG.

The paper is organized as follows. First, we identify the role of group velocity matching in 3D quantum simulations including *all* phase-mismatch effects. We observe that the HHG efficiency at long-wavelength, short driving pulses decreases due to GVM. Second, we consider the effect of GVM separately to study its role in HHG. To this end, we introduce a semiclassical definition of the walk-off length in HHG. Then, we validate our definition by comparing our model predictions with the results of quantum simulations at different driving wavelengths. We further show that GVM shows a preferential growth of harmonics generated by short trajectories, and leads to the isolation of an attosecond burst near the peak of the driving laser pulse. We study the scaling of GVM with driving wavelengths and pulse duration, demonstrating that GVM effects are largest for long wavelength driving lasers, and short pulse durations. Finally, we show that GVM affects the attosecond yield independent of the value of the carrier-envelope-phase (CEP) of the driver pulse.

2. Role of group velocity in time-gated phase-matching

To visualize the walk-off delay, associated with the group velocity, we show in figures 1(a1) and (b1) the driving field (in a frame moving at the speed of light) at the entrance (grey) and at the exit (red) of a 2 mm gas cell where the harmonics are generated, for a few-cycle (a) and a multi-cycle (b) driving laser. In the few-cycle case, the walk-off time delay imprinted in the envelope due to the group velocity (indicated in green) can be clearly seen. In contrast, in the case of a multi-cycle field, the fields at the entrance and exit are virtually indistinguishable, i.e. the walk-off delay is very small. As the harmonic phase is very sensitive to the electric field, it can be expected that the walk-off delay may substantially modify the macroscopic HHG signal for a few-cycle pulse. As we will show next, this is indeed the case for high harmonic and attosecond pulse generation at mid-IR wavelengths.

To this end, we have performed 3D numerical simulations, including *all* phase contributions: namely phase and group velocity, intrinsic as well as geometric phase, and also absorption. We model HHG including 3D propagation using the electromagnetic field propagator [25], and computing the single-atom dipole acceleration using the SFA+ approach [26], which has been validated against TDSE simulations [7, 26]. Note that we account for the time-dependent induced ionization population (computed via the instantaneous ADK rates [27, 28]), thus including nonlinear phase shifts in the driving field. Nonlinear spatial effects are not taken into account. We have considered a loose focusing geometry given by a Bessel beam of 60 μm in radius propagating into a 2 mm helium cell, selecting the harmonic radiation produced on-axis. Note that we have chosen helium because it allows us to extend the harmonic radiation to higher photon energies [3, 16, 17], but the results presented in this

work can be applied to other rare gases as well. The laser pulse is modeled as $E(t) = E_0 \sin^2(\pi t/2\sqrt{2}\,\tau_{\mathrm{p}})$ $\cos(2\pi ct/\lambda + \phi_{\mathrm{CEO}})$, with $\lambda = 2\,\mu$m, intensity FWHM pulse duration (a) $\tau_{\mathrm{p}} = 1.4$ cycles (9.3 fs) and (b) $\tau_{\mathrm{p}} = 5.8$ cycles (38.7 fs), and carrier-envelope offset (a) $\phi_{\mathrm{CEO}} = 0.25\pi$ and (b) $\phi_{\mathrm{CEO}} = 0$.

Figure 1 shows the scaling of the HHG yields from the 3D numerical simulations for (a) a few-cycle and (b) a multi-cycle driver pulse at $2\,\mu$m as a function of gas pressure. The peak intensities fulfill perfect phase-matching conditions at the center of the pulse [16] ((a) 4.96×10^{14} W cm^{-2}, and (b) 4.47×10^{14} W cm^{-2}). As a consequence, non-perfect phase–velocity matching at the wings of the laser pulse leads to a reduction of the number of attosecond bursts with increasing pressure (figures 1(a2) and (b2)). In contrast, the yield of the central pulse initially increases with pressure due to perfect phase–velocity matching, as it has been observed recently for long driving pulses [18]. Note also that the duration of the central pulse within the train (650 as FWHM), does not change with pressure for a multi-cycle driver (panel (b2)). However, for a few-cycle laser driver, we observe a reduction of the attosecond pulse yield at the highest pressures (panel (a2)), which appears independent of the choice of the CEP (see also section 2.4). In addition, the pulse duration is also reduced with increasing pressure.

To further analyze this effect, we show the integrated yield of the central pulse of the train as a function of the gas pressure in panels (a3) and (b3), when *all* phase matching contributions are considered (purple solid line), and when GVM is artificially removed (red dashed line). The results in panel (a3) show that the strong reduction of the harmonic yield for the few-cycle driver is unequivocally related to GVM. In contrast, the yield in panel (b3) increases with gas pressure due to a favorable GVM at long pulse durations. We emphasize that it has been experimentally demonstrated [3, 18] that bright soft x-ray harmonic generation and the isolation of high energy attosecond pulses can be obtained at long driver wavelengths and in the regime of perfect phase matching. Our simulations demonstrate the need of understanding the fundamental role of GVM in this important parameter regime.

3. Group velocity walk-off in HHG

In the previous section we have identified the relevance of GVM in HHG driven at long wavelengths and high pressures in numerical simulation including all contributions to a phase mismatch in HHG. In order further study the role of GVM in the HHG process, in this section we will deliberately neglect all phase mismatch effects except for GVM. We will proceed by providing first a definition of the walk-off length in terms of the semiclassical action at non-perturbative intensities and validate this definition by comparing its predictions with the results of numerical calculations. This will provide us with the opportunity to analyze the role of GVM as a function of wavelength and pulse duration as well as its dependence on the CEP.

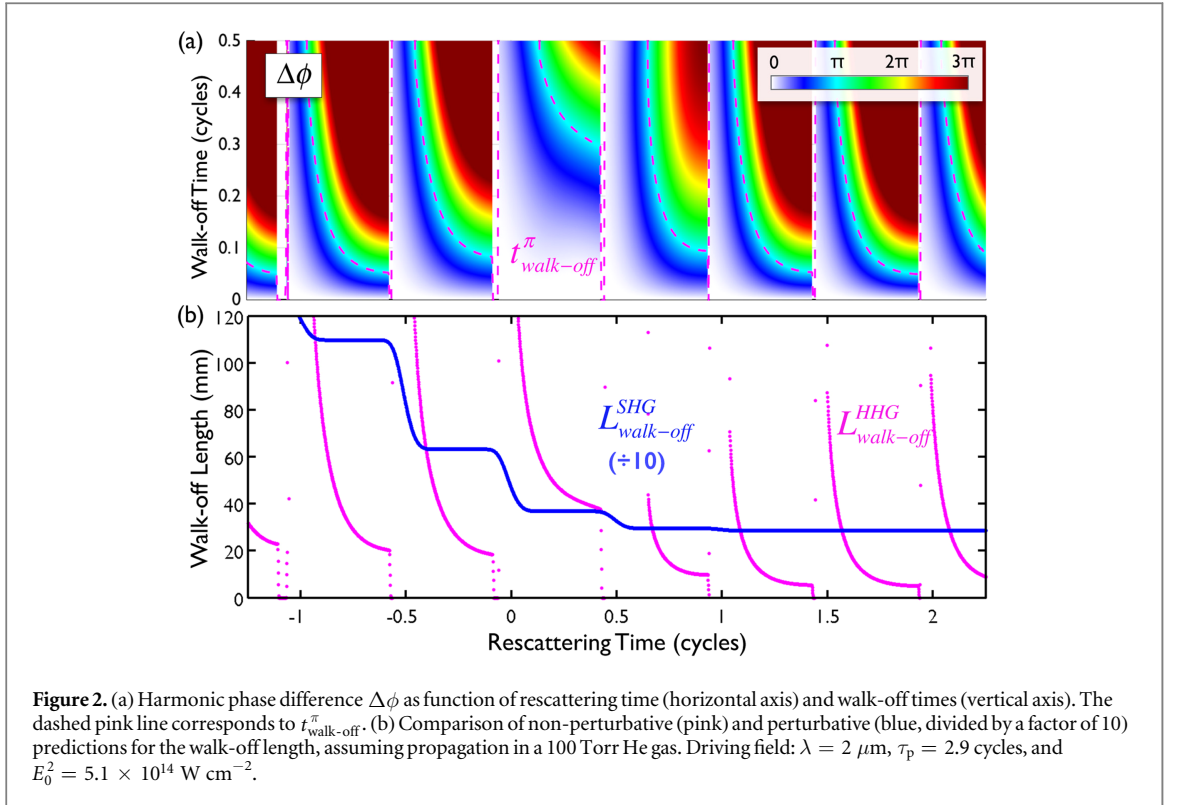### 3.1. Definition of semiclassical walk-off length
Phase matching in HHG is described in terms of the coherence length, which is defined as $L_{\mathrm{coh}}^{q} = \pi/\Delta k_q$, where Δk_q, is the phase mismatch of the qth order harmonic. It corresponds to the distance between two atoms in the target whose qth order harmonic emission interferes destructively.

In a loose focusing geometry or in a waveguide, the intrinsic HHG and geometric contributions to the phase mismatch can be neglected. Perfect phase–velocity matching conditions can be achieved via the compensation of the contributions to the refractive index from the free electrons and neutrals over significant propagation distances (i.e. longer than the absorption depth). In this case the phase of the fundamental field travels with the speed of light and the coherence length approaches infinity [16, 18]. However, due to the time-dependent ionization along the course of the pulse, perfect compensation can be achieved only during a finite temporal window. This effect can be observed at the central part of the pulse in figures 1(a) and (b), where the electric field propagates at the speed of light, c. Note that in the front part of the pulse phase-matching is governed by the neutrals, whereas in the rear part by the free electrons, thus imprinting an asymmetry in the electric field. Consequently, imperfect phase–velocity matching leads to the suppression of the attosecond harmonic bursts at the wings but not at the central cycle of the pulse.

Under these conditions, the group velocity, v_{g}, which is the velocity at which the envelope of the pulse travels, becomes an important factor. It is related to the phase velocity v_{ph} as

$$v_{\mathrm{g}}^{-1}(\lambda) = v_{\mathrm{ph}}^{-1}(\lambda) - \frac{\lambda}{c}\frac{\partial n_{\mathrm{R}}(\lambda)}{\partial \lambda}, \tag{1}$$

where n_{R} is the refractive index of the generating medium. Hence, the group velocity depends not only on the gas parameters (such as species and pressure) but may also change over the course of the pulse due to ionization induced by the pulse itself. In perturbative SHG in crystals, the walk-off length associated with GVM is defined as [22–24]

Figure 2. (a) Harmonic phase difference $\Delta\phi$ as function of rescattering time (horizontal axis) and walk-off times (vertical axis). The dashed pink line corresponds to $t^{\pi}_{\text{walk-off}}$. (b) Comparison of non-perturbative (pink) and perturbative (blue, divided by a factor of 10) predictions for the walk-off length, assuming propagation in a 100 Torr He gas. Driving field: $\lambda = 2\ \mu\text{m}$, $\tau_{\text{p}} = 2.9$ cycles, and $E_0^2 = 5.1 \times 10^{14}\ \text{W cm}^{-2}$.

$$L^{\text{SHG}}_{\text{walk-off}} = \frac{\tau_{\text{P}}}{|\Delta\nu_{\text{g}}^{-1}(\lambda_0,\ \lambda_0/2)|}, \tag{2}$$

where τ_{p} is the (FWHM) pulse width, $\Delta\nu_{\text{g}}^{-1}(\lambda_1,\ \lambda_2) = [\nu_{\text{g}}^{-1}(\lambda_1) - \nu_{\text{g}}^{-1}(\lambda_2)]$ and λ_0 is the central wavelength of the fundamental laser field. Accordingly, the temporal overlap between the pump and the second harmonic waves decreases significantly for propagation distances exceeding the walk-off length.

While such a definition is useful in the case of a perturbative low-order process such as SHG, it is not applicable for the non-perturbative and highly nonlinear process of HHG, since the phases of the high-order harmonics are sensitive to the actual electric field (phase and amplitude). We therefore propose a new definition of the walk-off length in HHG as

$$L^{\text{HHG}}_{\text{walk-off}} \simeq \frac{t^{\pi}_{\text{walk-off}}}{|\nu_{\text{g}}^{-1}(\lambda_0) - \nu_{\text{g}}^{-1}(\lambda_q)|}, \tag{3}$$

where $\nu_{\text{g}}(\lambda_q)$ is the group velocity of the qth harmonic. In the present work we have further approximated $\nu_{\text{g}}(\lambda_q) \simeq c$, i.e. the group velocity of the harmonics equals the speed of light, which is a reasonable assumption for the higher-order harmonics in the EUV and soft x-ray regime considered in our analysis below. $t^{\pi}_{\text{walk-off}}$ is the envelope walk-off time needed to imprint a shift of π in the intrinsic phase of the harmonic field. The walk-off time itself is defined as the time delay experienced by the pulse envelope propagating with ν_{g} over a distance z as compared to a propagation with the speed of light, i.e. $t_{\text{walk-off}} = z/\nu_{\text{g}}(\lambda_0) - z/c$. Analogous to the coherence length, one can interpret the walk-off length $L^{\text{HHG}}_{\text{walk-off}}$ as the distance between two atoms whose harmonic emission interferes destructively due to GVM.

In order to determine the walk-off time needed to imprint a phase-shift of π in the harmonics, we use the semiclassical analysis of HHG by Lewenstein *et al* [29]. The phase of the harmonic field can be written as $\phi = S(t,\ t_1)/\hbar$, where $S(t,\ t_1)$ is the semiclassical action of a free electron interacting with an electromagnetic field, $E(t)$, along the classical path ionized at t_1 with zero initial velocity, and leading to a rescattering at time t. This semiclassical formulation enables us to determine the phase difference $\Delta\phi(t_{\text{walk-off}})$ of the harmonic field generated by two (identical) laser pulses whose envelopes are delayed to each other by a walk-off time $t_{\text{walk-off}}$.

To validate our definition and analyze the effects of GVM, in model calculations we deliberately neglect all phase mismatch sources, i.e., $L^q_{\text{coh}} = \infty$. In figure 2(a) we show the phase difference $\Delta\phi$ as a function of the rescattering time and the walk-off time. The rescattering times are scaled with respect to the center of the laser pulse. Within each half-cycle different harmonics are emitted at different rescattering times depending on the kinetic energy upon recollision. The dashed pink line in figure 2(a) indicates the phase difference $\Delta\phi = \pi$, corresponding to $t^{\pi}_{\text{walk-off}}$. Assuming a 100 Torr helium cell and accounting for the time-dependent induced ionization population (computed via the instantaneous ADK rates [27, 28]), we show in figure 2(b) the
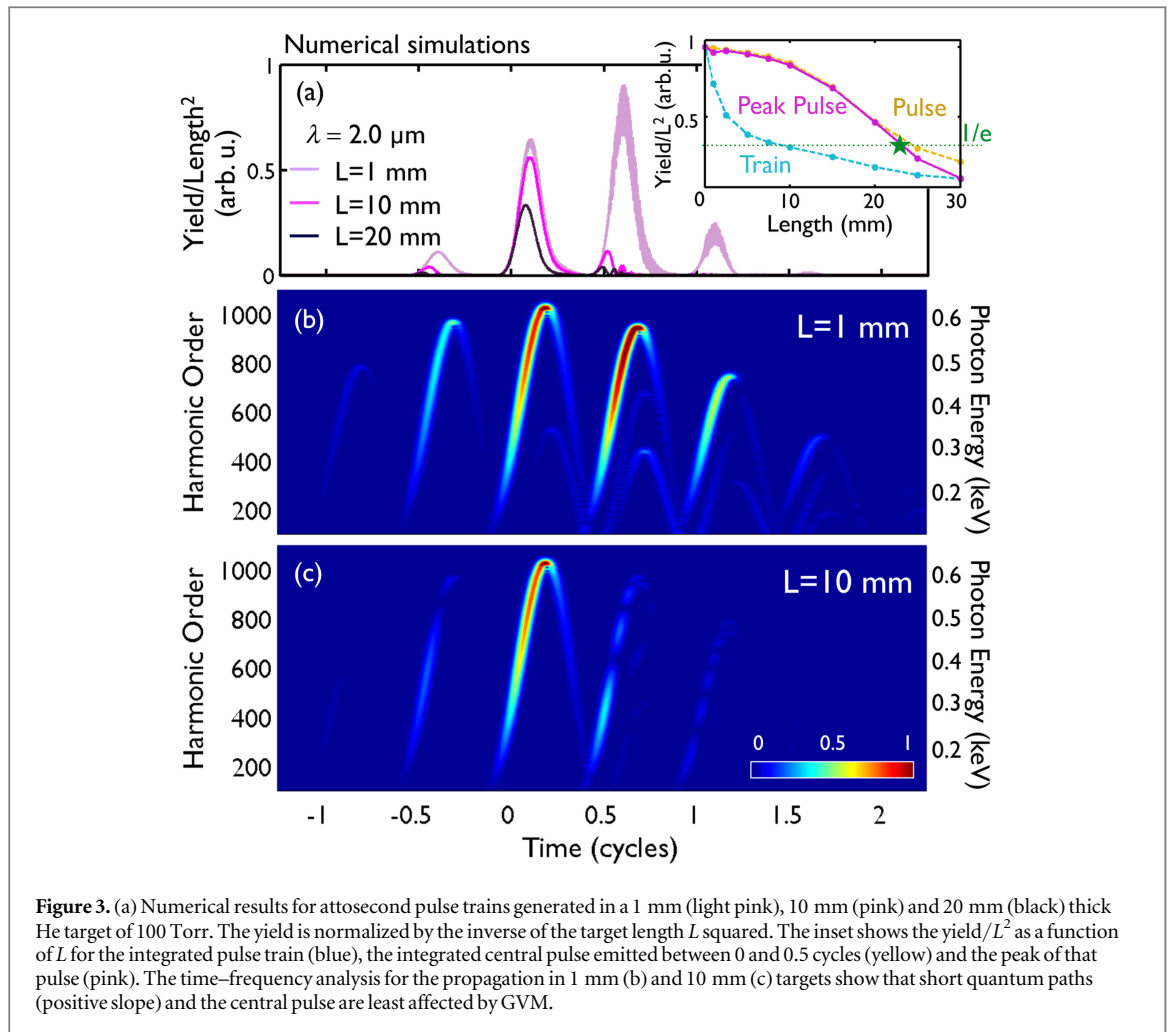
Figure 3. (a) Numerical results for attosecond pulse trains generated in a 1 mm (light pink), 10 mm (pink) and 20 mm (black) thick He target of 100 Torr. The yield is normalized by the inverse of the target length L squared. The inset shows the yield/L^2 as a function of L for the integrated pulse train (blue), the integrated central pulse emitted between 0 and 0.5 cycles (yellow) and the peak of that pulse (pink). The time–frequency analysis for the propagation in 1 mm (b) and 10 mm (c) targets show that short quantum paths (positive slope) and the central pulse are least affected by GVM.
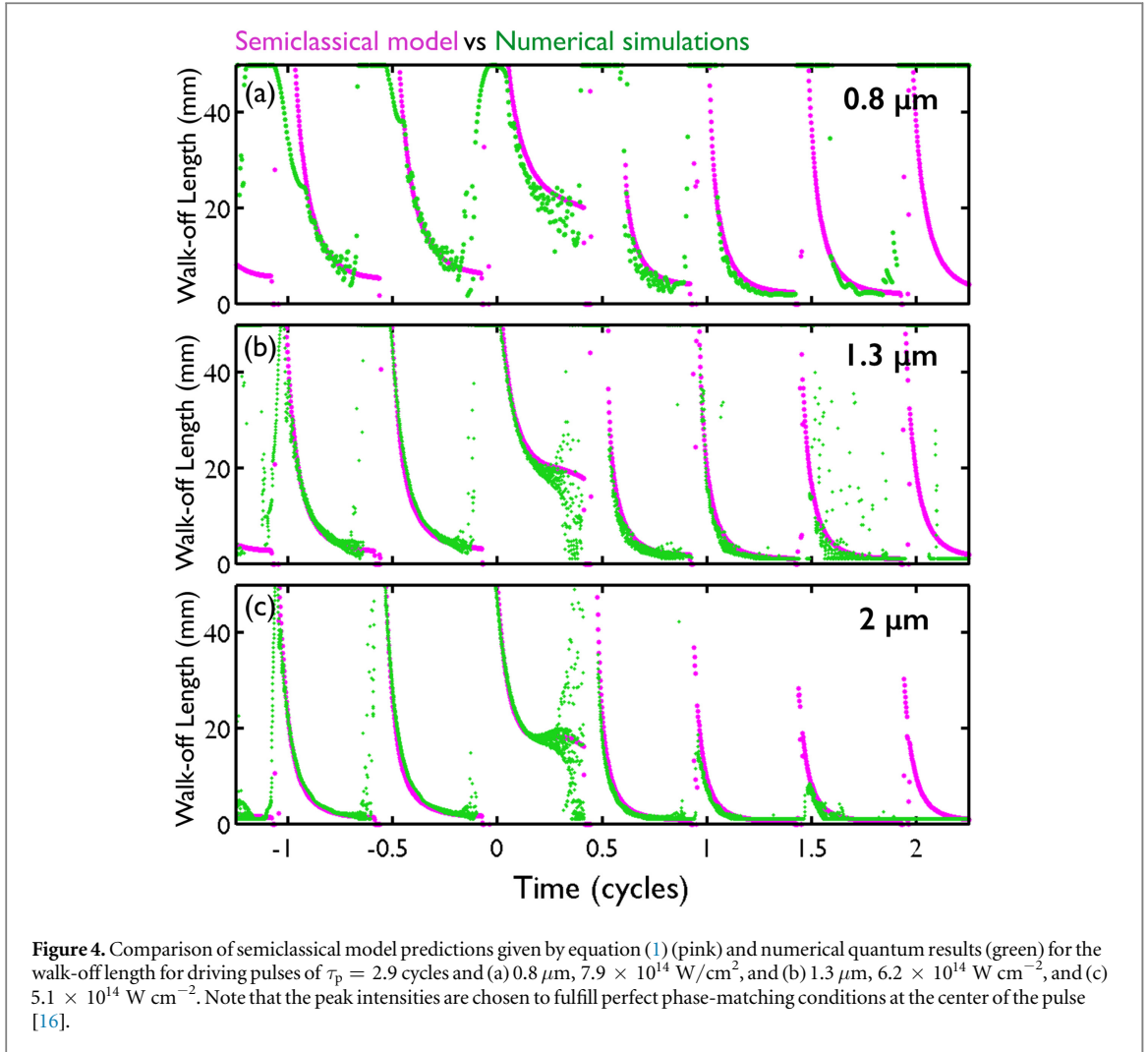
associated walk-off length $L_{\text{walk-off}}^{\text{HHG}}$ (pink line, see equation (3)). Note that $L_{\text{walk-off}}^{\text{HHG}}$ is significantly shorter than the perturbative walk-off length $L_{\text{walk-off}}^{\text{SHG}}$ (blue line, divided by a factor of 10 for comparison).

Two novel features concerning GVM in HHG can be seen from the results in figure 2. First, the walk-off length $L_{\text{walk-off}}^{\text{HHG}}$ is longest at the center of the driving laser pulse, where the time-derivative of the pulse envelope is lowest, in contradiction to the perturbative predictions, which steadily decrease from one half-cycle to the next. Furthermore, within each half-cycle $L_{\text{walk-off}}^{\text{HHG}}$ varies and decreases, thus the so-called *short* trajectory contributions will exhibit a better GVM than the *long* ones. This effect is a direct consequence of the HHG phase, whose intensity dependence is larger for *long* trajectory contributions [29]. In contrast, in the perturbative model, the walk-off length remains constant within each cycle and *short* and *long* trajectories would be equally affected by GVM.

3.2. Validation against quantum simulations

We now proceed to validate the definition of walk-off length against our full 3D numerical quantum simulations including propagation. We consider propagation in one dimension and model perfect phase-matching conditions by deliberately neglecting all mismatching effects, except GVM, as well as absorption in the electromagnetic field propagator [25]. In figure 3(a) we present the numerical results for the attosecond pulse trains generated in 1mm (light pink), 10 mm (pink) and 20 mm (black) thick helium target at a pressure of 100 Torr. In the simulations we used the same 2 μm driving laser pulse as for the semiclassical calculations shown in figure 2. In the case of perfect GVM the attosecond pulse yield is expected to increase with the square of the target length L. In order to demonstrate the mismatch effects, we therefore present yields/L^2 in figure 3(a). Figures 3(b) and (c) represent the time–frequency analysis of the radiation generated in 1 and 10 mm helium gas targets, respectively.

First, in the time–frequency analysis we observe the expected attosecond chirp [30, 31] of the short trajectory (positive slope) and long trajectory (negative slope) contributions. By comparing the two time–frequency plots one can observe that the results of the numerical quantum simulations agree with the general features predicted by the semiclassical model for GVM in HHG. While the yields in the central attosecond pulse are barely affected,

Figure 4. Comparison of semiclassical model predictions given by equation (1) (pink) and numerical quantum results (green) for the walk-off length for driving pulses of $\tau_p = 2.9$ cycles and (a) 0.8 μm, 7.9 $\times$ 10^{14} W/cm^2, and (b) 1.3 μm, 6.2 $\times$ 10^{14} W cm^{-2}, and (c) 5.1 $\times$ 10^{14} W cm^{-2}. Note that the peak intensities are chosen to fulfill perfect phase-matching conditions at the center of the pulse [16].
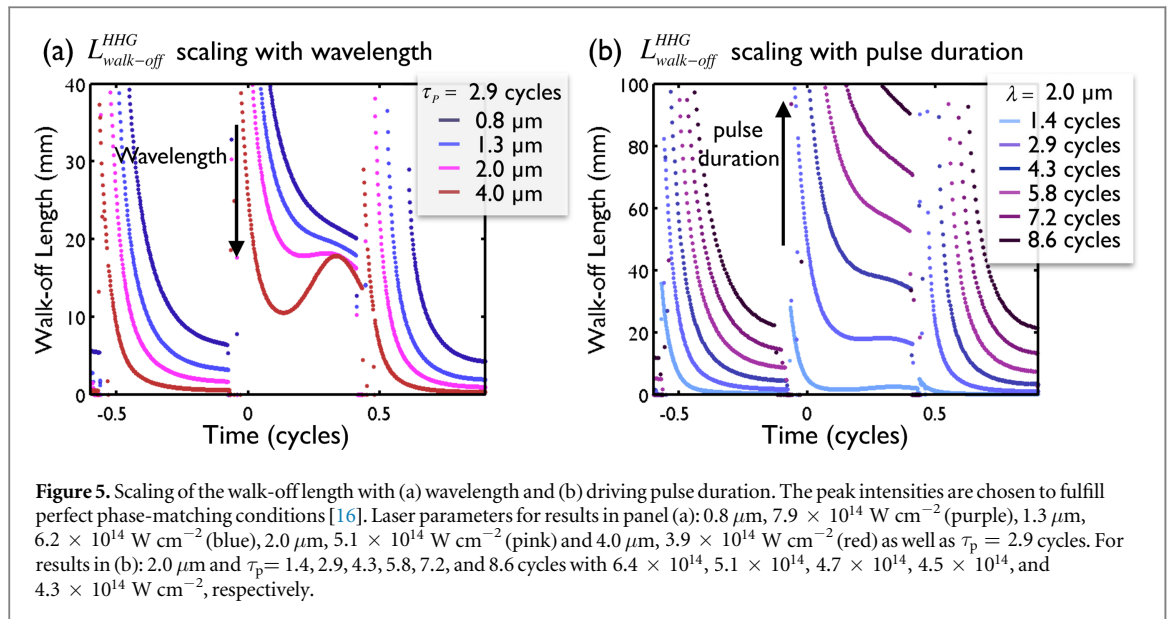
the other pulses are strongly suppressed for propagation in the longer target. This agrees with the model predictions that the walk-off length in HHG is longest at the center of the pulse. Furthermore, within each half-cycle of the field the contributions from the short trajectories (positive slope) are less affected by GVM than the long trajectories (negative slope), which agrees with the semiclassical model predictions that the walk-off length decreases within each half-cycle.

Next, we compare the numerical quantum results for the walk-off length with the semiclassical predictions, based on equation (3). We determine the walk-off length in the quantum results as the interaction length at which the peak pulse yield/L^2 drops by $1/e$ (see green star in the inset of figure 3(a)). The comparison between the semiclassical (pink) and the numerical (green) results is shown in figure 4 for (a) 0.8 μm, (b) 1.3 μm, and (c) 2.0 μm driving fields. The driving pulse duration is $\tau_p = 2.9$ cycles, and the peak intensities (E_0^2) are 7.9 $\times$ 10^{14} W cm^{-2}, 6.2 $\times$ 10^{14} W cm^{-2}, and 5.1 $\times$ 10^{14} W cm^{-2} respectively. The excellent agreement between the numerical and semiclassical results further confirms the validity of the semiclassical definition of the walk-off length for a broad wavelength regime.

3.3. Scaling with wavelength and pulse duration

We note that the walk-off length depends on the driving wavelength (see figure 4), therefore we present in figure 5(a) the model predictions for the corresponding scaling. For perfect phase matching intensities the group velocity difference $|\Delta v_g^{-1}|$ does not vary much with wavelength. However, $t_{\text{walk-off}}^\pi$ and the corresponding HHG walk-off length decreases, as can be seen in figure 5(a), since the harmonic phase in HHG is proportional to the excursion time of the electronic wave packet times the ponderomotive potential [29]. Thus, for a given (walk-off) time delay, GVM effects become more prominent for longer driving wavelengths. In contrast, at short wavelengths, absorption of the harmonics in the generating medium is more restrictive than GVM. For example, for the 100 eV harmonics generated in He (100 Torr) at 0.8 μm, the absorption length (L_{abs}, medium distance at which the transmitted intensity drops by $1/e$ [32]) is 3.6 mm [33], whereas the walk-off length extracted from figure 4(a) is $L_{\text{walk-off}}^{\text{HHG}} \simeq 30$ mm. However, the 500 eV harmonics generated at 2 μm have $L_{\text{abs}} = 410$ mm, and

Figure 5. Scaling of the walk-off length with (a) wavelength and (b) driving pulse duration. The peak intensities are chosen to fulfill perfect phase-matching conditions [16]. Laser parameters for results in panel (a): 0.8 μm, 7.9×10^{14} W cm^{-2} (purple), 1.3 μm, 6.2×10^{14} W cm^{-2} (blue), 2.0 μm, 5.1×10^{14} W cm^{-2} (pink) and 4.0 μm, 3.9×10^{14} W cm^{-2} (red) as well as $\tau_p = 2.9$ cycles. For results in (b): 2.0 μm and $\tau_p = 1.4$, 2.9, 4.3, 5.8, 7.2, and 8.6 cycles with 6.4×10^{14}, 5.1×10^{14}, 4.7×10^{14}, 4.5×10^{14}, and 4.3×10^{14} W cm^{-2}, respectively.

$L_{\text{walk-off}}^{\text{HHG}} \simeq 20$ mm. As a consequence, the yield of soft x-ray harmonics generated by long wavelength laser pulses is more restricted by GVM than absorption.

On the other hand, in figure 5(b) we analyze the scaling of the walk-off length in HHG with driving pulse duration τ_p. The semiclassical predictions for the walk-off length for a 2 μm driving laser pulse decrease for a decreasing pulse duration, again in agreement with the results of the full simulations (figure 1). This can be understood by the fact that a given walk-off delay in the envelope does have a stronger effect on the shape of the electric field in a short pulse than in a long pulse, as depicted in figures 1(a) and (b). This leads to the counterintuitive effect that at long driver wavelengths the generation of isolated attosecond pulses is more efficient in long driver pulses.
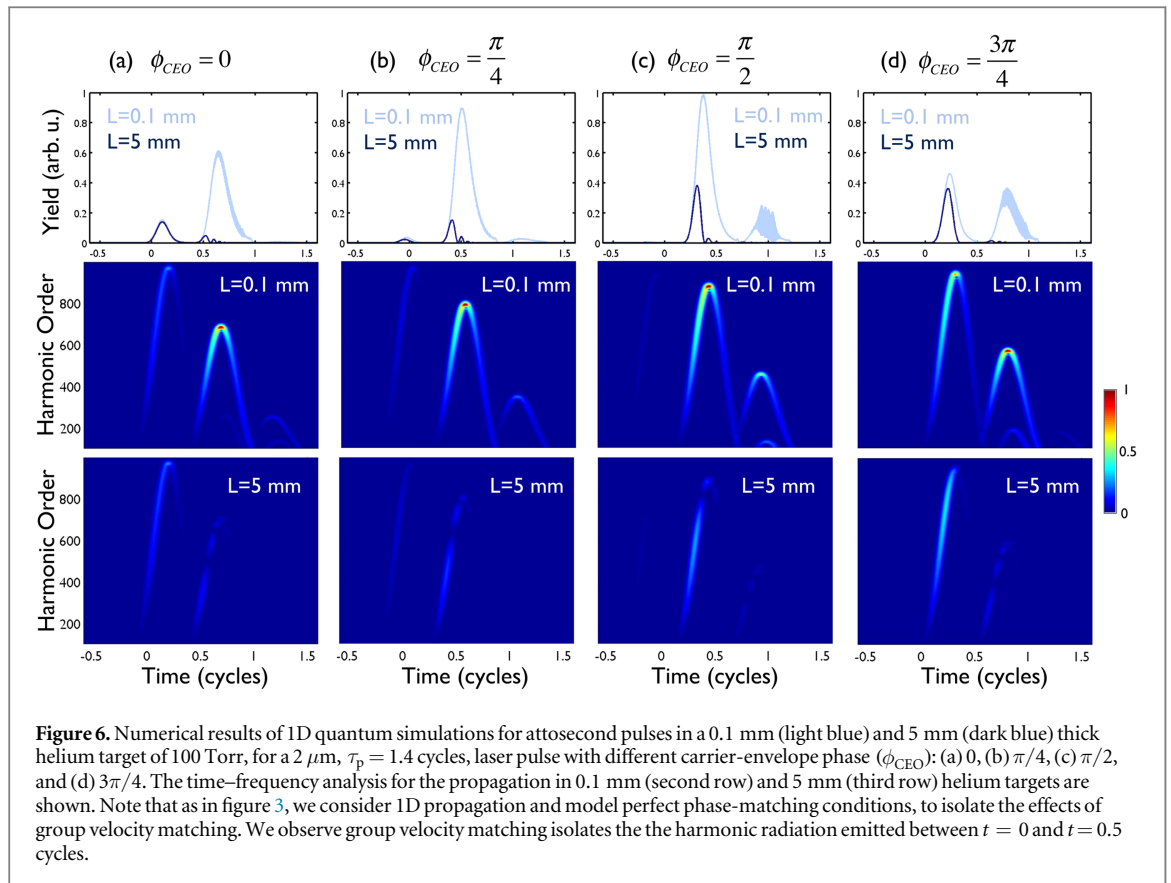
Finally, we noted that the pulse duration of the attosecond pulse generated by a few-cycle driver in figure 1(a2) is reduced with increasing pressure, in contrast to the multi-cycle driver (figure 1(b2)). We attribute this behavior to GVM. As stated in sections 3.1 and 3.2, the walk-off length decreases with the rescattering time of the HHG process. As a consequence, first the long trajectories and then the highest frequency components of the short trajectory contributions are suppressed, thus reducing the pulse duration, but also its frequency content.

3.4. CEP dependence

The results presented in figure 5(b) show that the walk-off length is particularly relevant for few-cycle laser pulses. It is therefore appropriate to study how the GVM effects depend on the CEP of the driving field. As in previous simulations in this section, to concentrate on the effect of GVM, we consider 1D quantum simulations neglecting all mismatching effects except GVM. In figure 6 we present the simulation results for a 2 μm, few-cycle ($\tau_p = 1.4$ cycles) laser pulse with CEP (ϕ_{CEO}) of: (a) 0, (b) $\pi/4$, (c) $\pi/2$, and (c) $3\pi/4$. In the first row we present the attosecond pulses generated in 0.1 mm (light blue), and 5 mm (dark blue) thick helium target at a pressure of 100 Torr. In order to identify the mismatch effects, we represent the time–frequency analysis of the radiation generated in 0.1 mm (second row) and 5 mm (third row) helium gas targets, respectively. It can be clearly observed that, no matter the driving-CEP value, only the harmonic radiation emitted between $t = 0$ and $t = 0.5$ cycles is group-velocity matched. Therefore, group velocity matching affects the attosecond yield for every value of the driving-CEP.

4. Conclusions

Based on results of numerical simulations including all phase matching effects, we have shown that group velocity matching plays a relevant role for high harmonic generation with driver pulses at long mid-IR wavelengths and short durations. The effect of group velocity matching has been analyzed by providing a definition of the walk-off length associated with GVM in HHG. Model predictions corresponding to this definition are shown to be in excellent agreement with results of quantum simulations. It is further shown that GVM contributes to the isolation of attosecond pulses and the suppression of the contributions from long quantum paths. Our theoretical results also indicate that group velocity matching contributes to a restriction of

Figure 6. Numerical results of 1D quantum simulations for attosecond pulses in a 0.1 mm (light blue) and 5 mm (dark blue) thick helium target of 100 Torr, for a 2 μm, $\tau_p = 1.4$ cycles, laser pulse with different carrier-envelope phase (ϕ_{CEO}): (a) 0, (b) $\pi/4$, (c) $\pi/2$, and (d) $3\pi/4$. The time–frequency analysis for the propagation in 0.1 mm (second row) and 5 mm (third row) helium targets are shown. Note that as in figure 3, we consider 1D propagation and model perfect phase-matching conditions, to isolate the effects of group velocity matching. We observe group velocity matching isolates the the harmonic radiation emitted between $t = 0$ and $t = 0.5$ cycles.

the efficiency of the generation of isolated attosecond pulses with short pulses in the long driver wavelength regime.

Acknowledgments

References

[1] McPherson A, Gibson G, Jara H, Johann U, Luk T S, McIntyre I A, Boyer K and Rhodes C K 1987 *J. Opt. Soc. Am.* B **4** 595
[2] Ferray M, L'Huillier A, Li X F, Lompre L A, Mainfray G and Manus C 1988 *J. Phys. B: At. Mol. Opt. Phys* **21** L31
[3] Popmintchev T *et al* 2012 *Science* **336** 1287
[4] Christov I P, Murnane M M and Kapteyn H C 1997 *Phys. Rev. Lett.* **78** 1251
[5] Paul P M, Toma E S, Breger P, Mullot G, Augé F, Balcou P, Muller H G and Agostini P 2001 *Science* **292** 1689
[6] Kienberger R *et al* 2004 *Nature* **427** 817
[7] Hernández-García C, Pérez-Hernández J A, Popmintchev T, Murnane M M, Kapteyn H C, Jaroń-Becker A, Becker A and Plaja L 2013 *Phys. Rev. Lett.* **111** 033002
[8] Schafer K J, Yang B, DiMauro L F and Kulander K C 1993 *Phys. Rev. Lett.* **70** 1599
[9] Corkum P B 1993 *Phys. Rev. Lett.* **71** 1994
[10] Gaarde M B, Tate J L and Schafer K J 2008 *J. Phys. B: At. Mol. Opt. Phys* **41** 132001
[11] Popmintchev T, Chen M C, Arpin P, Murnane M M and Kapteyn H C 2010 *Nat. Photon* **4** 822
[12] Salières P, L'Huillier A and Lewenstein M 1995 *Phys. Rev. Lett.* **74** 3776
[13] Balcou P, Salières P, L'Huillier A and Lewenstein M 1997 *Phys. Rev.* A **55** 3204
[14] Hernández-García C and Plaja L 2012 *J. Phys. B: At. Mol. Opt. Phys* **45** 074021
[15] Rundquist A R, Durfee C G III, Chang Z, Herne C, Backus S, Murnane M M and Kapteyn H C 1998 *Science* **280** 1412

[16] Popmintchev T, Chen M C, Bahabad A, Gerrity M, Sidorenko P, Cohen O, Christov I P, Murnane M M and Kapteyn H C 2009 *Proc. Natl Acad. Sci. USA* **106** 10516
[17] Chen M C, Arpin P, Popmintchev T, Gerrity M, Zhang B, Seaberg M, Murnane M M and Kapteyn H C 2010 *Phys. Rev. Lett.* **105** 173901
[18] Chen M-C *et al* 2014 *Proc. Natl Acad. Sci. USA* **111** E2361
[19] Austin D R and Biegert J 2014 *New J. Phys.* **16** 113011
[20] Comly J and Garmire E 1968 *Appl. Phys. Lett.* **12** 7
[21] Glenn W 1969 *IEEE J. Quantum Electron.* **QE-5** 284–90
[22] Weiner A M 1983 *IEEE J. Quantum Electron.* **QE-18** 1276
[23] Eckardt R C and Reintjes J 1984 *IEEE J. Quantum Electron.* **QE-20** 1178
[24] Hayata K and Koshiba M 1993 *Appl. Phys. Lett.* **62** 2188
[25] Hernández-García C, Pérez-Hernández J A, Ramos J, Conejero Jarque E, Roso L and Plaja L 2010 *Phys. Rev. A* **82** 033432
[26] Pérez-Hernández J A, Roso L and Plaja L 2009 *Opt. Express* **17** 9891
[27] Amosov M V, Delone N B and Krainov V P 1986 *Zh. Eksp. Teor. Fiz.* **91** 2008
[28] Becker A and Faisal F H M 2005 *J. Phys. B: At. Mol. Opt. Phys* **38** R1
[29] Lewenstein M, Balcou P, Ivanov M Y, L'Huillier A and Corkum P B 1994 *Phys. Rev. A* **49** 2117
[30] Mairesse Y *et al* 2003 *Science* **302** 1540–3
[31] Sansone G *et al* 2006 *Science* **314** 443–6
[32] Constant E, Garzella D, Breger P and Mével E 1999 *Phys. Rev. Lett.* **82** 1668–71
[33] Henke B L, Gullikson E M and Davis J C 1993 *At. Data Nucl. Data Tables* **54** 181–342